Intermediate-velocity atomic collisions. IV. Ar K-shell ionization and capture by C^{5+} and C^{6+} ions

E. C. Montenegro,* Xiang-Yuan Xu,† W. E. Meyerhof, and R. Anholt‡
Department of Physics, Stanford University, Stanford, California 94305
(Received 19 February 1988)

Ar K x rays produced by 22- and 42-MeV C^{5+} and C^{6+} ions were measured in coincidence with the various emergent charge states resulting from the collision process. Single-electron K-shell capture and ionization cross sections are obtained through an analysis based on the independent-particle model (IPM). The comparison among various theoretical models and the present experiment shows that the present theoretical description of the electron capture is more precarious than that of ionization in the intermediate-velocity regime studied. The IPM analysis also allows one to obtain estimates of the probability of C^{5+} electron loss for small-impact-parameter collisions.

I. INTRODUCTION

In previous papers (I–III) (Refs. 1–3) on atomic collisions in the intermediate velocity region, we studied projectile ionization and capture in various gases by C and Ca ions with few electrons. Projectile ionization is appropriate to study binding and polarization effects in this regime because the Pauli principle closes the capture channels into the occupied target states. As a consequence, the ionization and capture processes are isolated from each other and a transparent comparison between theory and experiment can be achieved. In our previous experiments, electron capture was studied without selection of the initial target states. Although this reveals important features of the capture process in many-electron atoms such as the velocity matching condition (III),[3] the contribution from some particular target shell cannot be analyzed in detail. On the other hand, our coincidence measurements (II,III) (Refs. 2 and 3) provided a comprehensive view of the role played by the final projectile states, including the formation of metastables states in heliumlike ions such as Ca^{18+}.

In the present work a specific selection of the target active electron was achieved. The K-shell x-ray production of Ar by C^{5+} and C^{6+} projectiles was studied by making coincidence measurements between the Ar K X rays and the emerging projectile charge states. Two projectiles velocities (v_p) were used: 8.56 and 11.8 (in a.u., which will hereafter be used). With this choice, $Z_p < v_p < Z_t$ (Z_p and Z_t are the atomic numbers of the projectile and the target, respectively) and the intermediate-to-low–velocity regime for the Ar K-shell ionization and capture was explored.

The study of atomic collisions in which multielectronic processes are involved is of great interest at present.[4–11] The simplest theoretical model used in these studies is the independent-particle model (IPM) which neglects electron-electron interactions. This model is expected to give a reasonable description of multiple-ionization and capture processes involving inner-shell electrons because of the small contribution due to electron-electron interaction when compared to the potentials of the collision partners. In this work the IPM was used to interpret the experimental measurements. Although the main objective of this work is to obtain single-electron cross sections for K-shell ionization and capture, the experiment inevitably mixes in multielectron processes. For example, the K-shell single capture process is mixed with the K-shell ionization-L-shell capture double electron process. This channel cannot be neglected because $v_p \simeq Z_t/2$ and L-shell capture is then very likely for the system studied.

As in the previous papers of this series, we compared our K-shell capture results with the eikonal approximation.[1,12] We also have examined the strong-potential Born approximation[13] which gives good agreement with experiment for K-shell capture by protons with the same velocities as used in this work. The ionization results were compared to the Glauber approximation[2,14,15] and the molecular-orbital–plane-wave Born approximation (MO-PWBA) theory.[16,17] We also used the estimate of Matveev[18] to calculate the probability of loss of C^{5+}, which is necessary to extract the ionization and capture cross sections from the data.

Section II of this paper describes the experimental techniques used. The approximations developed within the IPM to obtain the ionization and capture cross sections are presented in Sec. III. Section IV makes comparisons with different theories for K-shell ionization and capture. Section V presents a summary of the main conclusions.

II. EXPERIMENTAL METHODS

Figure 1 shows schematically the apparatus used in this experiment. The selected C^{5+} or C^{6+} beam from the Stanford FN Van de Graaf accelerator was sent into a

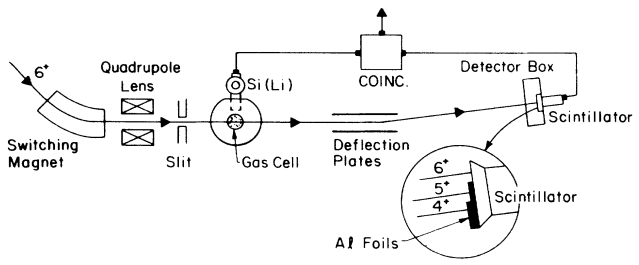

FIG. 1. Schematic diagram of the experimental apparatus used.

0.8-cm-long differentially pumped gas cell after it had passed through a quadrupole lens and the collimating slits. The emerging charge states from the gas cell were analyzed by 80-cm-long deflection plates with about 10 kV of voltage and directed into the detector box.

The detector box housed one parallel plate avalanche counter (PPAC) and one scintillation counter. The PPAC is described in detail in paper I (Ref. 1) and was used to check the present charge state ratios with those obtained in I. The coincidence measurements were carried out with the scintillator, using basically the same technique described in papers II (Ref. 2) and III (Ref. 3). Nevertheless, instead of dividing the scintillator in two sections as before, we separated the sensitive area of the scintillator in three portions in order to detect three charge states simultaneously (Fig. 1). Two of these portions were covered with Al foils with different thicknesses and the other portion was kept uncovered. The relative positions of the covered sections were changed with the incident charge state to give the highest pulse height for the most intense charge state measured, so that pileup would not falsify the weaker charge state counts. Each section was 13 mm wide in the plane defined by the primary and secondary beams. By using the quadrupole lens and the slits, a beam spot with less than 1.0 mm diameter was obtained at the position of the scintillator and each section was carefully scanned to ensure that each charge state hit the center of the corresponding section.

Beam collimation by the slits and focusing assured that the entrance and exit apertures of the gas cell were not hit. As a consequence, a clean Ar K x-ray peak was obtained when the 16-mm-diam Si(Li) detector was placed into the gas cell at 90° with respect to the incident beam.

The signals from the scintillator together with those the Si(Li) detector were sent to fast-slow coincidence electronics and into a computer based data acquisition system. The counting rate in the scintillator was kept below 10 Kcounts/s during all the measurements.

The present experiment was done with pressures of 0.2 and 0.4 Torr in the gas cell. At these pressures, all the secondary charge states had an intensity less than 10% of the intensity of the primary charge state. The residual pressure in the beam line was less than 2×10^{-6} Torr which gives a negligible contribution to charge change of the primary beam. Further details of gas cell, pressure measurement, and pumping system can be found in I.[1]

The absolute values of the cross sections presented in this paper were determined through a normalization factor obtained from a 3.5-MeV $p+$Ar ionization measurement under the same conditions described above. The cross section adopted for the normalization was 6.1 Kb as given by the Glauber,[14,15] MO-PWBA (Refs. 16 and 17) and ECPSSR (Ref. 19) theories. These three theories give almost the same value for this cross section. For the present work with C projectiles, the use of protons for cross-section normalization assumes that the Ar fluorescence yield is only little affected by L- and M-shell multiple ionization. The main sources of uncertainty in our experiment come from the measurement of target pressure, the charge exchange between the exit of the gas cell and the entrance of the deflection plates and the counting statistics which also affect the selection of the windows for sorting the coincidence spectra. An average uncertainty of ±30% should be assigned to the values of the cross sections reported in this work.

III. DATA ANALYSIS AND RESULTS

Table I presents the experimental results for the Ar K-shell vacancy production cross section $\sigma(i,f)$ as a function of the C initial (i) and final (f) charge states.

As mentioned above, multielectronic processes can give a sizeable contribution to the measured cross section $\sigma(i,f)$. In order to extract from $\sigma(i,f)$ the single-electron ionization and capture cross sections we proceed with an analysis based on the IPM. We use the following notation: σ_1 is the one-electron Ar K-shell ionization cross section (by any C ion); σ_i^{1c} is the one-electron Ar K-shell capture cross section by a C ion with charge state i; $P_1(b)$ is the one-electron Ar K-shell ionization probability as a function of the impact parameter b; $P_{iK}^{1c}(b)$ is the one-electron capture probability from the Ar K shell by a C ion with charge state i as a function of the impact parameter b; $P_{iLM}^{1c}(b)$ is the one-electron capture probability from the Ar $L+M$ shells by a C ion with charge state i as a function of impact parameter b; and $P_{\rm loss}(b)$ is the probability of electron loss of C^{5+} as a function of b.

In paper I,[1] it was shown that the most important contribution to one-electron capture of C^{6+} ions in Ar in this velocity range, $v_p \simeq Z_t/2$, comes from the Ar L and M shells. As a first approximation, we can then neglect K-shell electron capture compared to L- and M-shell capture. We also neglect, as a first estimate, multielectron processes comprising more than two target electrons. This assumption is justified by the observation in Table I that $\sigma(6,4)$, which is related to double capture, is 8% and 17% (for 22 and 42 MeV, respectively) of $\sigma(6,5)$, which is related to single capture. Hence, processes which result in an Ar K vacancy and involve more than two electrons are expected to be of minor importance.

With these assumptions, the cross sections $\sigma(i,f)$ can be written as

$$\sigma(6,6)=2\pi\int_0^\infty b\,db\,P_1(b)[1-P_{6LM}^{1c}(b)]\,, \tag{1}$$

$$\sigma(6,5)=2\pi\int_0^\infty b\,db[P_{6K}^{1c}(b)+P_1(b)P_{6LM}^{1c}(b)]\,, \tag{2}$$

$$\sigma(6,4)=2\pi\int_0^\infty b\,db\,P_{6K}^{1c}(b)P_{6LM}^{1c}(b)\,, \tag{3}$$

TABLE I. Measured Ar K-shell vacancy production cross section $\sigma(i,f)$ as a function of C initial (i) and final (f) charge states. Units are $10^5 b$. (All cross sections are normalized using a 3.5-MeV proton beam and have a relative uncertainty of ±30%.).

	22 MeV		42 MeV	
	i			
f	5	6	5	6
4	0.08	0.09	0.4	0.4
5	0.9	1.3	2.0	2.3
6	0.6	0.7	1.3	2.3

$$\sigma(5,6)=2\pi\int_0^\infty b\,db\,P_{\rm loss}(b)P_1(b)[1-P^{1c}_{6LM}(b)]\ , \quad (4)$$

$$\sigma(5,5)=2\pi\int_0^\infty b\,db\{[1-P_{\rm loss}(b)]P_1(b)[1-P^{1c}_{5LM}(b)] + P_{\rm loss}(b)[P^{1c}_{6K}(b) + P_1(b)P^{1c}_{6LM}(b)]\}\ , \quad (5)$$

$$\sigma(5,4)=2\pi\int_0^\infty b\,db\{[1-P_{\rm loss}(b)] \times[P^{1c}_{5K}(b)+P_1(b)P^{1c}_{5LM}(b)] + P_{\rm loss}(b)P^{1c}_{6K}(b)P^{1c}_{6LM}(b)\}\ . \quad (6)$$

The integrands of Eqs. (1)–(6) are linear in $bP_1(b)$, $bP^{1c}_{6K}(b)$, or $bP^{1c}_{5K}(b)$. Because the collision regime is such that the projectile velocity is about one-half of the Ar K-shell Bohr velocity, these functions reach their maximum value at impact parameters smaller than the Ar K-shell radius. Consequently, the collision preferentially scans the inner region of the Ar L and M wave functions. The same can be said for the C K-shell wave function. Following this reasoning, a further simplification of Eq. (1)–(6) can be made by substituting for $P_{\rm loss}(b)$ and $P^{1c}_{iLM}(b)$ their values at $b=0$. The cross sections $\sigma(i,f)$ can then be written as

$$\sigma(6,6)\simeq\sigma_1[1-P^{1c}_{6LM}(0)]\ , \quad (7)$$

$$\sigma(6,5)\simeq\sigma^{1c}_6+\sigma_1P^{1c}_{6LM}(0)\ , \quad (8)$$

$$\sigma(6,4)\simeq\sigma^{1c}_6P^{1c}_{6LM}(0)\ , \quad (9)$$

$$\sigma(5,6)\simeq\sigma_1P_{\rm loss}(0)[1-P^{1c}_{6LM}(0)]\ , \quad (10)$$

$$\sigma(5,5)\simeq\sigma_1[1-P_{\rm loss}(0)][1-P^{1c}_{5LM}(0)] + P_{\rm loss}(0)[\sigma_1P^{1c}_{6LM}(0)+\sigma^{1c}_6]\ , \quad (11)$$

$$\sigma(5,4)\simeq[1-P_{\rm loss}(0)][\sigma^{1c}_5+\sigma_1P^{1c}_{5LM}(0)] + \sigma^{1c}_6P_{\rm loss}(0)P^{1c}_{6LM}(0)\ . \quad (12)$$

Equations (7)–(12) give some insight into the results presented in Table I. If $P_{\rm loss}(0)$ is set equal to unity, we have $\sigma(6,6)\simeq\sigma(5,6)$, $\sigma(6,5)\simeq\sigma(5,5)$ and $\sigma(6,4)\simeq\sigma(5,4)$. These results are generally corroborated by Table I and have a simple physical meaning: collisions in which an Ar K x ray is emitted, highly perturb the C^{5+} electron, resulting in a large probability of electron loss. As a consequence, approximately the same cross section $\sigma(i,f)$ is obtained no matter what the incident charge state is.

Equations (7)–(12) represent two sets of measurements corresponding to the 6+ [(Eq. (7)–(9)] and 5+ [(Eq. (10)–(12)] charge states. We solved this system of equations by successive approximations. The first set was solved separately and the second set was solved by minimizing the sum of the squared differences for the parameters which are common to the two sets. Table II presents the results obtained for σ_1, σ^{1c}_6, $P^{1c}_{6LM}(0)$, and $P_{\rm loss}(0)$.

Because the probability of loss is large, the quantities σ^{1c}_5 and $P^{1c}_{5LM}(0)$ do not have a large influence in Eqs. (11) and (12). As a consequence, and also due to the experimental uncertainties, these two quantities cannot be determined with a sufficient precision to warrant a detailed discussion (they are omitted from Table II). For the other quantities, it can be seen from Table II that the results obtained with the 6+ and 5+ beams agree with each other within the experimental uncertainties, supporting the present method of analysis and the procedures adopted. In Sec. IV, we proceed with a detailed analysis of these parameters by comparison with various theories for K-shell capture and ionization.

TABLE II. Inferred quantities from the analysis based on the independent-particle model. (Typical uncertainties for inferred quantities are ±30% for C^{6+} and ±35% for C^{5+}.)

	$\sigma_1(10^5b)$	Ar $\sigma^{1c}_6(10^5b)$		$P^{1c}_{6LM}(0)$		C $P_{\rm loss}(0)$
		i[a]				
E (MeV)	5	6	5	6	5	6	5
22	0.8	0.8	0.9	1.2	0.07	0.07	0.8
42	2.4	2.8	1.6	1.8	0.16	0.16	0.7

[a]Initial C charge states.

IV. DISCUSSION

A. K-shell ionization cross sections

Figure 2 compares the measured Ar K-shell ionization cross sections with Glauber[2,14,15] and MO-PWBA (Refs. 16 and 17) calculations for C^{6+}. The Glauber calculation is described in the previous papers (I,II).[1,2] The MO-PWBA model uses the adiabatic perturbation theory to determine the $1s\sigma$ molecular orbital ionization cross section at low projectile velocities ($v_p \ll Z_t$) and provides the necessary matching with the PWBA at higher velocities through the introduction of an effective charge. This effective charge simulates the relaxation of the active and passive electrons (binding effect) and connects this relaxation to the evolution of the center of charge during the collision process (static polarization).[16,17,20] Figure 2 shows that the MO-PWBA reproduces well the trend of the experimental data while the Glauber approximation gives too high values at low velocities.

In paper II we studied Ca K-shell ionization for a projectile velocity near the velocity of the active electron. It was shown that both Glauber and PWBA (with a binding correction based on the MO-PWBA model) give a good description of the experimental data. In the present work, the collision regime is such that the projectile velocity is about one half of the active electron velocity and, as Fig. 2 shows, this condition apparently sets a limit to the applicability of Glauber calculations.

B. K-shell electron capture cross sections

Figure 3 compares the measured Ar K-shell single-electron capture cross sections with the eikonal[1,12] and SPB (Ref. 13) calculations. The SPB values were obtained by making a simple Z_p^5 scaling to calculated p+Ar

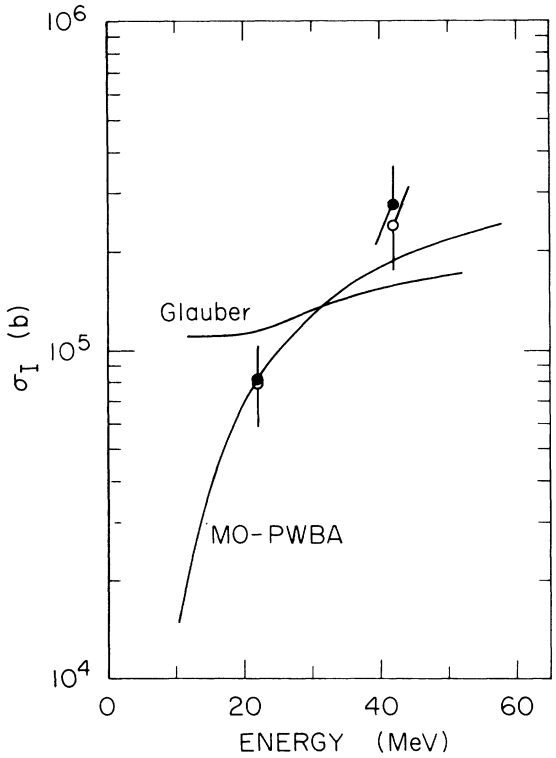

FIG. 2. Ar K-shell ionization cross sections by C^{6+} and C^{5+} projectiles. Theoretical curves: MO-PWBA and Glauber approximations (see text). Experimental points are from this work: (●), C^{6+}; (○), C^{5+}. Cross sections are in units of barns.

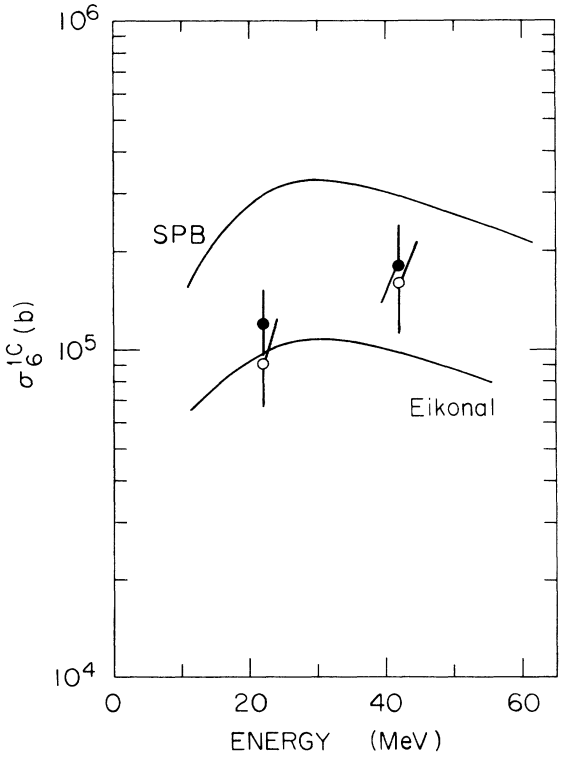

FIG. 3. Ar K-shell electron capture cross sections by C^{6+} and C^{5+} projectiles. Theoretical curves: SPB and eikonal approximations (see text). Experimental points are from this work: (●), C^{6+}; (○), C^{5+}.

K-shell capture cross sections.[13] The contribution to capture into all the projectiles states was taken into account through a multiplicative factor 1.2 given by the $1/n^3$ scaling law.[13] The eikonal cross sections were determined following the same procedures as described in paper III.[3]

As mentioned above, the SPB approximation gives good agreement with experiment for $p+\mathrm{Ar}$ in this velocity range. The Z_p^5 scaling applied to C projectiles changes the proton capture cross sections by almost four orders of magnitude, resulting in cross sections which are about a factor of 2 larger than the values experimentally obtained. Thus the Z_p^5 scaling appears to be roughly applicable. As a matter of fact, a factor $Z_p^{4.6}$ gives a good agreement with the present experiment. A similar behavior was observed by Rødbro *et al.*[21] in their measurements of K-shell capture of Ne and C by p, He^{2+}, and Li^{3+} projectiles. Their results clearly show that increasing Z_p results in capture cross sections which are progressively smaller than those predicted by Z_p^5 scaling.

It should be noted that in the regime studied by this work ($Z_p < v_p < Z_t$) the SPB is the only approximation that can be justifiably used.[22] The full peaking SPB calculations have a more restricted validity[22] ($v_p^3 \gg Z_p Z_t^2$), while the eikonal calculations are valid only if $v_p \gg Z_t$. Hence, the curves presented in Fig. 3 should be considered as theoretical guides to obtain order of magnitude estimates.

C. K-shell vacancy production cross section

The experimental study of K-shell vacancy production cross section (σ_v) is in general simpler than the corresponding ionization or capture because it does not involve the use of coincidence techniques. The cross section σ_v is obtained without making any selection among the emergent charge states of the projectile. For example, in the C^{6+} beam case, σ_v is given by

$$\sigma_v = \sum_f \sigma(6,f) \ . \tag{13}$$

This can be compared with other noncoincidence measurements of K x-ray production cross sections. Our cross sections, obtained from Eq. (13) by summing over the three measured charge states are presented in Fig. 4 together with the results of Refs. 23 and 24. The conversion from the x-ray production cross sections given by Ref. 24 to σ_v was made by means of the fluorescence yield $\omega_K = 0.118$.[25] It can be seen from Fig. 4 that our measured points agree well with the other data, supporting our data analysis and normalization procedures.

Theoretical estimates of σ_v can be obtained combining Eq. (13) with Eqs. (7)–(9). As a first approximation we can write

$$\sigma_v \simeq \sigma(6,6)+\sigma(6,5) = \sigma_1 + \sigma_6^{1c} \ , \tag{14}$$

which gives σ_v in terms of the one one-electron ionization and capture cross sections described in the preceding sections.

Figure 4 shows the resulting values of σ_v (solid curve)

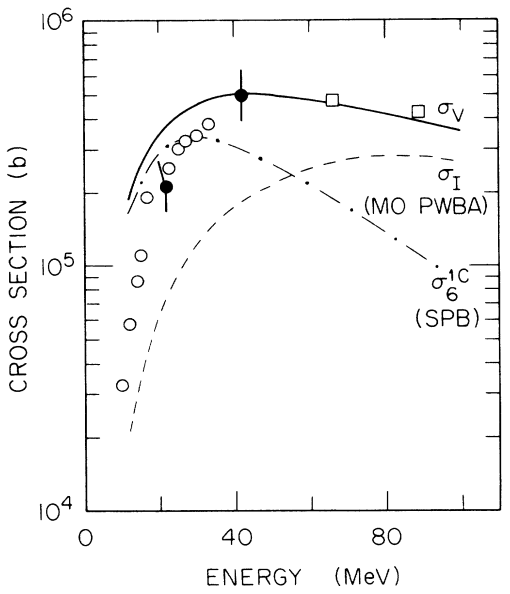

FIG. 4. Ar K-shell vacancy production cross sections. Experimental data: (●), this work; (○) and (□) taken from Refs. 23 and 24. Theory: (— — —), σ_1, MO-PWBA; (—·—·—·), σ_6^{1c}, SPB; (——), σ_v, Eq. (14).

when the MO-PWBA (dashed curve) and SPB (dashed-dotted curve) theories are used to calculate σ_1 and σ_6^{1c} respectively. For higher velocities, where the ionization dominates, the calculated σ_v presents good agreement with the experimental data. At lower energies, the theoretical calculations give a predominance of the capture process. This result is not supported by our experimental σ_1 and σ_6^{1c} results at 22 MeV (see Figs. 2 and 3), where approximately the same value was found for these two cross sections. It is also interesting to note that the experimental values of σ_v decrease sharply when the projectile energy falls below 40 MeV. This behavior is well followed by the MO-PWBA model for K-shell ionization. On the other hand, the theoretical models for electron capture give a much weaker energy dependence than that of experimental σ_v data for projectile energies below 20 MeV.

D. Probability of C^{5+} electron loss

In the analysis based on the IPM presented in Sec. II, we obtained the quantity $P_{\rm loss}(0)$, which is the probability of loss of the C^{5+} electron during the Ar K-shell ionization or capture process. Although this quantity was obtained in an indirect way, a theoretical estimate will be made to check the consistency of the approximations adopted.

The C^{5+} projectile ionization by Ar is, in the present situation, a high-velocity, highly perturbative collision. For this system, the SCA approximation[26] gives ionization probabilities larger than unity, which is an indication that the large values of $P_{\rm loss}(0)$ found (see Table II) are indeed expected. Recently, Matveev[18] developed a simple model that can be applied to the present situation. Translated to our projectile ionization case, the model states that if the target (Ar) electric field is sufficiently strong and v_p sufficiently high ($v_p \gg Z_p$), the C^{5+} electron can be viewed as a wave packet performing a classical Rutherford scattering in the field of Z_t. As a result, the C^{5+} electron receives a sudden momentum transfer $q=2v_p\sin(\theta/2)$ (θ is the classical electron c.m. scattering angle) without changing appreciably its position relative to the C nucleus. The transition amplitude is then given by[18]

$$A_n(q)=\int d^3r\,\Psi_n^*(r)\Psi_0(r)\exp(i\mathbf{q}\cdot\mathbf{r})\ , \tag{15}$$

with $\Psi_n^*(r)$ and $\Psi_0(r)$ being, respectively, the final and initial states wave functions of the C^{5+} electron.

Equation (15) is now applied to compute the probability of loss. Following the analysis of Sec. III, the probability of loss $P_{\rm loss}(0)$ should be determined at zero *nuclear* impact parameter. Under these conditions, the *electronic* wave packet undergoes a Rutherford scattering at an impact parameter $\simeq 1/Z_p$, which results in a c.m. scattering angle Θ such that cotan $\Theta/2\simeq v_p^2/Z_pZ_t$. This scattering angle corresponds to a momentum transfer q_1 which allows the determination of $P_{\rm loss}(0)$ through the equation

$$P_{\rm loss}(0)=\sum_n |\,A_n(q_1)\,|^2\ , \tag{16}$$

where the summation is carried out over all the final (continuum) states.

Noting that the integration and the summation in Eqs. (15) and (16) are the same that appear in the PWBA theory for the ionization cross section,[27] we can determine $P_{\rm loss}(0)$ by

$$P_{\rm loss}(0)=\int_1^\infty dw\,|\,F_w(Q_1)\,|^2\ , \tag{17}$$

where

$$F_w(Q_1)=\frac{2^7}{1-\exp(2\pi/k)}\frac{Q_1(Q_1+k^2/3+1/3)}{[(Q_1-k^2+1)^2+4k^2]^3}\times\exp\{-(2/k)\arctan[2k/(Q_1-k^2+1)]\}\ , \tag{18}$$

$$Q_1=(q_1/Z_p)^2=(2v_p/Z_p)^2/[1+(v_p^2/Z_pZ_t)^2]\ , \tag{19}$$

and

$$w=k^2+1\ . \tag{20}$$

Here, w is the energy transfer in atomic units divided by Z_p^2.

Figure 5 compares the results of these calculations with the values of $P_{\rm loss}(0)$ given in Table II. It can be seen that reasonable agreement is obtained, suggesting that Ar K-shell ionization and electron capture by C^{5+} ions are indeed likely to be followed by C^{5+} electron loss.

A further check of the above calculations can be performed by determining the total cross section for electron loss, $\sigma_{\rm loss}$. Following the same reasoning as that of Ref. 18 (integrating over the momentum transfer) it can be shown that

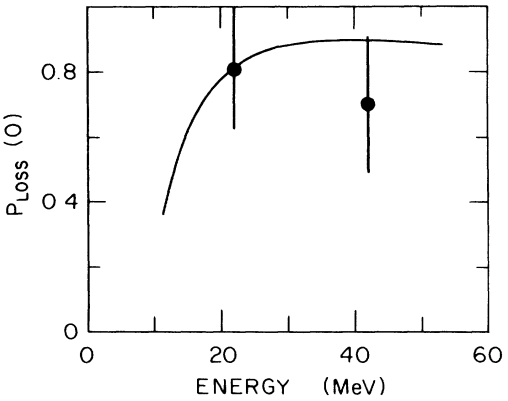

FIG. 5. Probability of loss by C^{5+} projectiles. The solid curve is based on the Matveev model (see text). Experimental points are from this work.

$$\sigma_{\text{loss}}=\frac{4\pi}{v_p^2}\frac{Z_t^2}{Z_p^2}\int_{w_{\min}}^{\infty}dw\int_{Q_0}^{Q_1}\frac{dQ}{Q^2}\,|F_w(Q)|^2\,, \tag{21}$$

with

$$Q_0=(2v_p/Z_p)^2[1+(v_p/Z_p)^4]\,.$$

We introduced two modifications in Eq. (21). First, the upper integration limit Q_1 was set equal to infinity. This change does not affect the regime $v_p \gg Z_p$ and $Z_t \gg Z_p$ in which the model applies, but, because it incorporates the higher momentum components of the momentum wave function, it allows the calculations to be extended towards slower collisions. Second, we introduced the binding correction in the same way as in paper II.[2] The minimum energy transfer $w_{\min}$ was set equal to $\bar{\varepsilon}$ where

$$\bar{\varepsilon}=\left[1+\frac{Z_t}{Z_p}g(\xi)\right]^2 \tag{22}$$

and $\xi=2v_p/Z_p$. With these modifications, σ_{loss} is given by

$$\sigma_{\text{loss}}=\frac{4\pi}{v_p^2}\frac{Z_t^2}{Z_p^2}\int_{\bar{\varepsilon}}^{\infty}dw\int_{Q_0}^{\infty}\frac{dQ}{Q^2}\,|F_w(Q)|^2\,. \tag{23}$$

Figure 6 compares our previous experimental results for σ_{loss} [paper I (Ref. 1)] with those given by Eq. (23) (solid curve) and Glauber calculations[1] (dashed curve). Although the present calculations are expected to be valid only for $Z_t \gg Z_p$, good agreement with the experiment is obtained for $Z_t \geq 8$. The Glauber approximation gives a better general description of the σ_{loss} data, but the model of Ref. 18 is much simpler to evaluate and may be used to advantage if the collision is sufficiently asymmetric or a simple estimate is needed for near symmetric collisions.

It should be noted that because Q_0 is independent of Z_t, the dependence of $\sigma_{\text{loss}}/Z_t^2$ on Z_t comes from the parameter $\bar{\varepsilon}$. Thus when Z_t increases, Eq. (23) associates directly the observed strong decrease of $\sigma_{\text{loss}}/Z_t^2$ to the transient (MO) binding energy of the system.

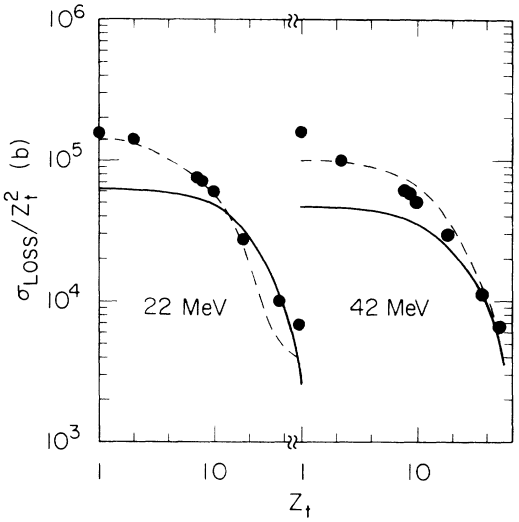

FIG. 6. Total cross section for C^{5+} electron loss in Ar. Experimental data are from paper I. The solid curve is based on the Matveev model (see text). The dashed curve is the Glauber calculation from paper I (Ref. 1).

E. Probability of capture from the Ar higher shells

Another quantity which emerges from the IPM analysis of Sec. II and deserves some remarks is $P_{6LM}^{1c}(0)$. This is a troublesome quantity to evaluate theoretically in the present energy region and the analysis below is limited to a qualitative examination of its energy dependence.

As discussed in paper I,[1] the major contribution to the total cross section $\sigma_{6,5}$ in the present energy region comes from the Ar L- and M-shell electrons [we use $\sigma_{6,5}$ to denote the total electron-capture cross section and $\sigma(6,5)$ as the capture cross section in coincidence with Ar K x rays]. Because $P_{6LM}^{1c}(0)$ also involves the Ar L- and M-shell electrons, we should expect, at least at first sight, that $P_{6LM}^{1c}(0)$ is closely related to $\sigma_{6,5}$ and follows a similar energy dependence. Nevertheless, in this energy region, $\sigma_{6,5}$ *decreases* with increasing energy ($\sigma_{6,5}=13$ and 2.7 Mb for 22 and 42 MeV, respectively)[1] while $P_{6LM}^{1c}(0)$ *increases* when the energy is increased (see Table II). We illustrate below, and in Fig. 7, a possible explanation of this effect. Our data is not sufficiently accurate to provide a definite experimental proof of the explanation.

Before analyzing the energy dependence of $P_{6LM}^{1c}(0)$ as compared with $\sigma_{6,5}$, we recall from Fig. 8 of paper I (Ref. 1) that for 42-MeV $C^{6+}+Ar$, the eikonal approximation predicts dominant electron capture from the $2p$ subshell. We can then assume, as a first estimate, that the major contribution to $P_{6LM}^{1c}(b)$ comes from the Ar $2p$ electrons for all values of b. If $p_{6LM}^{c}(b)$ is the electron capture probability *per electron* (assumed to be the same for all the Ar $2p$ electrons), the binomial distribution gives for the probability of capturing just one electron:

$$P_{6LM}^{1c}(b)\simeq 6p_{6LM}^{c}(b)[1-p_{6LM}^{c}(b)]^5\,. \tag{24}$$

The inclusion of the Ar $2s$ electrons (which adds some contribution to the electron capture at small impact pa-

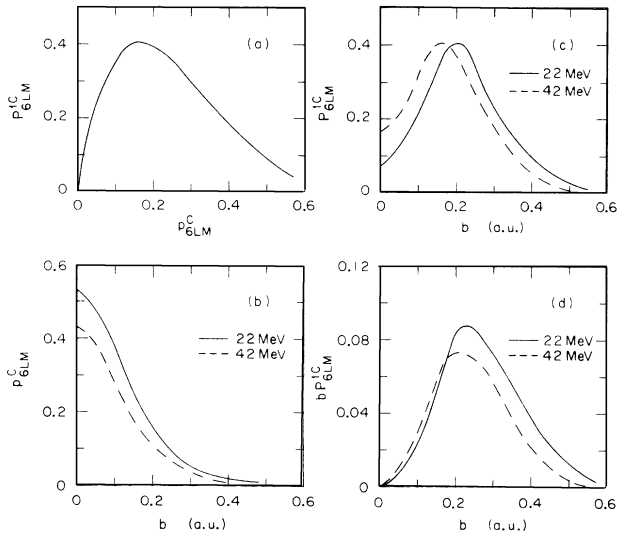

FIG. 7. Qualitative estimates of one-electron-capture probabilities from Ar L and M shells (see text). (a) Relationship between P^{1c}_{6LM} and p^{c}_{6LM} as given by the binomial distribution. (b) Probability of capture *per electron* as a function of the impact parameter b (in atomic units). (c) Probability to capture only one electron from Ar L and M shells as a function of b (normalized at $b=0$ to the values of Table II). (d) Curves obtained from (c) by multiplying $P^{1c}_{6LM}(b)$ by b. The area under the curves is proportional to the cross section $\sigma_{6,5}$ (see text).

rameters) does not change the main qualitative reasoning below.

Figures 7(a)–7(d) present, in an almost self-explanatory way, the proposed origin of the above-mentioned inversion of the energy dependence of $P^{1c}_{6LM}(0)$ as compared with $\sigma_{6,5}$. Figure 7(a) shows the relationship between $P^{1c}_{6LM}(b)$ and $p^{c}_{6LM}(b)$ as given by Eq. (24). This relationship is nearly linear if $p^{c}_{6LM}(b)$ is sufficiently small, a condition which is fulfilled whether the perturbation is small or the impact parameter is large (regardless the strength of the perturbation). In cases where $p^{c}_{6LM}(b)$ is large, $P^{1c}_{6LM}(b)$ becomes small due to the restriction imposed by the one-electron capture condition.

Figure 7(b) shows the shape of $p^{c}_{6LM}(b)$ for 22- and 42-meV C^{6+} projectiles. The curves were obtained on the basis of the OBK approximation,[11]

$$p^{c}_{6LM}(b)\simeq p^{c}_{6LM}(0)\left[\frac{y^2K_2(y)}{2}\right]^2 , \tag{25}$$

where $y=b\sqrt{\gamma}$;

$$\gamma=[v_p^4+2v_p^2(Z_p^2+Z_t^2/2)+(Z_p^2-Z_t^2/2)^2]/4v_p^2 ,$$

and $p^{c}_{6LM}(0)$ was obtained from the values of $P^{1c}_{6LM}(0)$ given in Table II using Eq. (24). It can be seen from Fig. 7(b) that for all impact parameters, $p^{c}_{6LM}(b)$ at 22 MeV is larger than for 42 MeV.

Figure 7(c) shows the one-electron-capture probability obtained from Eqs. (24) and (25). The inversion at small impact parameters occurs because the probability of capture *per electron* for 22-MeV projectiles is large and, as a consequence, the probability to capture just one electron becomes small. At large impact parameters the capture probability per electron becomes small and $P^{1c}_{6LM}(b)$ and $p^{c}_{6LM}(b)$ are related in an approximately linear way.

Finally, Fig. 7(d) shows why the inversion presented in Fig. 7(c) has a small influence on the total electron capture cross section $\sigma_{6,5}$, which is given by

$$\sigma_{6,5}=2\pi\int_0^\infty b\,dbP^{1c}_{6LM}(b) . \tag{26}$$

The product $bP^{1c}_{6LM}(b)$ is not sensitive to the differences between the values of $P^{1c}_{6LM}(b)$ for 22 and 42 MeV at small impact parameters. Consequently, $\sigma_{6,5}$ follows the same energy dependence as the capture probability per electron $p^{c}_{6LM}(b)$, which at large impact parameters is nearly equal to $P^{1c}_{6LM}(b)$.

V. CONCLUSIONS

In the present work, we studied Ar K-shell ionization and electron capture by C ions with high charge states in the intermediate velocity region. The projectile energies used are such that the resulting ionization or electron-capture cross section are scanned around their peak values, and towards the low-energy region.

Although this experiment selected the emergent charge state in coincidence with the target K x rays, this is insufficient to completely isolate the K-shell ionization and electron-capture processes from each other. Two-electron processes involving K and L- or M-shell electrons, which result in the same emergent charge state as the single-electron process, prevent the direct determination of the single-electron cross sections from the experimental observations. As a consequence, some additional assumptions based on the IPM were made in order to extract the single-electron cross sections.

Despite these difficulties, some interesting results could be obtained from our analysis based on the IPM. Besides determining the single-electron ionization and capture cross sections, it was possible to show that the probability of C^{5+} electron loss is very large if this ion participates in Ar K-shell vacancy production. Also, the IPM shows how the completely different behavior with the projectile energy of $\sigma_{6,5}$ and $P^{1c}_{6LM}(0)$ are, in fact, compatible. Although some of our conclusions are only qualitative, the analysis allows a comprehensive understanding of the system under investigation.

The theoretical scenario in the regime studied is essentially different for the ionization and electron-capture processes. For ionization, relatively simple calculations based on the plane-wave Born approximation (such as the MO-PWBA discussed in Sec. IV A) give good agreement

with the experiment. The same is not true for the electron-capture cross sections. There is at present no theory for inner-shell electron capture which can provide a satisfactory description of the intermediate-velocity regime. Also, experimental electron-capture data for this regime are scarce and this conjunction of factors prevents any deeper analysis of this process at present.

ACKNOWLEDGMENTS

This work was supported in part by the National Science Foundation under Grant No. 86-14650. E. C. M. acknowledges support from the Conselho Nacional de Desenvolvimento Científico e Technológico (CNPq) (Brazil).

*On leave from Pontifícia Universidade Católica do Rio de Janeiro, Brazil.

†Permanent address: Department of Physics, Tsinghua University, Beijing, People's Republic of China.

‡Present address: Gateway Modeling, Inc., Minneapolis, MN 55414.

[1]R. Anholt, X.-Y. Xu, Ch. Stoller, J. D. Molitoris, W. E. Meyerhof, B. S. Rude, and R. J. McDonald, Phys. Rev. A **37**, 1105 (1988).

[2]X.-Y. Xu, E. C. Montenegro, R. Anholt, K. Danzmann, W. E. Meyerhof, A. S. Schlachter, B. S. Rude, and R. J. McDonald, Phys. Rev. A **38**, 1848 (1988).

[3]E. C. Montenegro, X.-Y. Xu, W. E. Meyerhof, R. Anholt, K. Danzmann, A. S. Schlachter, B. S. Rude and R. J. McDonald, Phys. Rev. A **38**, 1854 (1988).

[4]A. Müller, B. Schuch, W. Groh, E. Salzborn, H. F. Beyer, P. H. Mokler, and R. E. Olsen, Phys. Rev. A **33**, 3010 (1986).

[5]M. Horbatsch and R. M. Dreizler, Z. Phys. D **2**, 183 (1986).

[6]W. E. Meyerhof, R. Anholt, X.-Y. Xu, H. Gould, B. Feinberg, R. J. McDonald, H. E. Wegner, and P. Thieberger, Phys. Rev. A **35**, 1967 (1987).

[7]R. D. Dubois and S. T. Manson, Phys. Rev. A **35**, 2007 (1987).

[8]J. H. McGuire, E. Salzborn, and A. Müller, Phys. Rev. A **35**, 3265 (1987).

[9]R. Gayet and A. Salin, J. Phys. B **20**, L577 (1987).

[10]R. Anholt, W. E. Meyerhof, X.-Y. Xu, H. Gould, B. Feinberg, R. J. McDonald, H. E. Wegner, and P. Thieberger, Phys. Rev. A **36**, 1586 (1987).

[11]D. P. Almeida, N. V. de Castro Faria, F. L. Freire, Jr., E. C. Montenegro, and A. G. de Pinho, Phys. Rev. A **36**, 16 (1987).

[12]J. Eichler, Phys. Rev. A **32**, 112 (1985).

[13]J. Macek and S. Alston, Phys. Rev. A **26**, 250 (1982).

[14]J. E. Golden and J. H. McGuire, Phys. Rev. A **12**, 82 (1975).

[15]J. H. McGuire, Phys. Rev. A **16**, 143 (1982).

[16]E. C. Montenegro and G. M. Sigaud, J. Phys. B **18**, 299 (1985).

[17]E. C. Montenegro, A. G. de Pinho, and G. M. Sigaud, J. Phys. B **19**, 3287 (1986).

[18]V. I. Matveev, Zh. Eksp. Teor. Fiz. **89**, 2021 (1985) [Sov. Phys.—JETP **62**, 1164 (1985)].

[19]D. D. Cohen and M. Harnigan, At. Data Nucl. Data Tables **33**, 255 (1985).

[20]G. M. Sigaud, E. C. Montenegro, J. Seidel, and M. Dost, Phys. Rev. A **34**, 4428 (1986).

[21]M. Rødbro, E. Horsdal-Pedersen, C. L. Cocke, and J. R. MacDonald, Phys. Rev. A **19**, 1936 (1979).

[22]K. Taulbjerg, in *Fundamental Processes in Energetic Atomic Collisions,* Vol. 103 of *NATO Advanced Study Institute, Series B: Physics* edited by H. O. Lutz, J. S. Briggs, and H. Kleinpoppen (U. S. GPO, Washington, D. C., 1982), p. 349.

[23]E. Salzborn, J. Guffey, L. D. Ellsworth, and J. R. MacDonald, Bull. Am. Phys. Soc. **20**, 639 (1975).

[24]H. Tawara, Y. Awaya, Y. Katow, M. Akiba, and M. Tonuma, Phys. Lett. **59A**, 14 (1976).

[25]M. O. Krause, J. Phys. Chem. Ref. Data **8**, 307 (1979).

[26]J. M. Hansteen, O. M. Johnsen, and L. Kocbach, At. Data Nucl. Data Tables **15**, 306 (1975).

[27]M. R. C. McDowell and J. P. Coleman, *Introduction to the Theory of Ion-Atom Collisions* (North-Holland, Amsterdam, 1970), p. 323.